Polyakov–Nambu–Jona-Lasinio phase diagrams and quarkyonic phase from order parameters

M. Dutra,[1] O. Lourenço,[2] A. Delfino,[3] T. Frederico,[1] and M. Malheiro[1]

[1]*Departamento de Física, Instituto Tecnológico de Aeronáutica, DCTA, 12.228-900 São José dos Campos, São Paulo, Brazil*

[2]*Departamento de Ciências da Natureza, Matemática e Educação, CCA, Universidade Federal de São Carlos, 13600-970 Araras, São Paulo, Brazil*

[3]*Instituto de Física - Universidade Federal Fluminense, Avenida Litorânea s/n, 24210-150 Boa Viagem, Niterói, Rio de Janeiro, Brazil*

(Received 29 August 2013; published 3 December 2013)

We show that the magnitude of the order parameters in the Polyakov–Nambu–Jona-Lasinio (PNJL) model given by the quark condensate and the Polyakov loop can be used as a criterion to clearly identify, without ambiguities, phases and boundaries of the strongly interacting matter, namely, the broken/restored chiral symmetry and confinement/deconfinement regions. This structure is represented by the projection of the order parameters in the temperature-chemical potential plane, which allows a clear identification of pattern changes in the phase diagram. Such a criterion also enables the emergence of a quarkyonic phase even in the two-flavor system. We still show that this new phase diminishes due to the influence of an additional vector-type interaction in the PNJL phase diagrams and is quite sensitive to the effect of the change of the T_0 parameter in the Polyakov potential. Finally, we show that the phases and boundaries constructed by our method indicate that the order parameters should be more strongly correlated, as in the case of the entanglement PNJL model. This result suggests a novel way to pursue further investigation of new interactions between the order parameters in order to improve the PNJL model.

DOI: 10.1103/PhysRevD.88.114013 PACS numbers: 12.38.Mh, 25.75.Nq

I. INTRODUCTION

In the large distances, or equivalently, low energies regime, one of the methods to treat quantum chromodynamics (QCD) is the numerical lattice calculations [1] based on Monte Carlo simulations [2]. The results from these techniques are provided for the pure gluon sector, i.e., in the limit of infinitely heavy quarks, as well as for systems including dynamical quarks. The latter systems, however, face the fermion sign problem [3] at the finite quark chemical potential (μ_q) regime. Nevertheless, such a problem is circumvented by reweighting methods, density of state ones, and others, see Refs. [4–8] for such treatments. Different from this method, another approach to describe QCD is the use of effective models such as the MIT bag model [9] and the Nambu–Jona-Lasinio (NJL) one [10–12]. The former treats gluons and massless quarks as free particles in which the confinement phenomenon is incorporated by including a bag constant in an *ad hoc* fashion. The latter presents further similarities with the full QCD theory but does not take into account the confinement, since quarks interact each other via pointlike interactions without exchanged gluons.

In order for the NJL model to become more realistic and taking into account the quark confinement at low energies, Fukushima [13] developed the Polyakov–Nambu–Jona-Lasinio model (PNJL), in which the confinement is included in the NJL structure through the Polyakov loop $\Phi = e^{-F_q/T}$, where F_q stands for the quark free energy (in Ref. [14], it is argued that Φ can be also represented by hadronic states). From this widely studied effective QCD model [15–28], much information on the strongly interacting matter can be obtained, such as its phase diagram [29], where the proper broken/restored chiral symmetry and confinement/deconfinement regions are identified. Other typical approaches are the use of two equations of state [30] in the description of the quark phase and the hadronic one [31], as well as hybrid models [32]. Moreover, other effective models coupled to the Polyakov loop are equally useful [33–38].

Different ways based on different criteria to construct the phase diagram in the $T \times \mu_q$ plane are addressed in the literature. In this work we compare such criteria and present a new criterion in order to clearly identify the regions and boundaries of the quark phase diagram generated exclusively from the PNJL model. Our analysis suggests that the order parameters should be correlated as in the entanglement PNJL model if the coincidence seen for the chiral and confinement transitions obtained from lattice QCD calculations at high T and very small μ_q is also confirmed for small temperatures and larger quark densities' values. This investigation follows a sequence of studies presented by our group in previous works [39,40], all of them motivated by the search of a better description of phases and boundaries of strongly interacting matter, specifically through analysis of PNJL phase diagrams.

The regime of high μ_q and very low temperatures is very important to investigate the existence of quark matter in the core of neutron stars or even in bare quark stars [41], one of the most important questions nowadays concerning the internal matter composition of compact stars, in particular, if the quarkyonic phase is presented or not. Therefore, our findings are useful, for instance, in the study of protoneutron stars that are described at $T < 50$ MeV. Applications

of PNJL models to compact stars have been done recently for the protoneutron stars' evolution [42,43], for quarks [44], and for hybrid stars [45]. Furthermore, we also point out that investigations of the quark phase diagram are relevant for a deeper understanding of the strongly interacting matter. The predictions of such studies, especially at the high density regime, will be tested in future experiments [46,47].

The paper is organized as follows. In Sec. II the basic thermodynamical quantities of the PNJL model are presented along with the distinct Polyakov potentials used in the literature. In Sec. III we discuss the PNJL phase diagrams constructed from different criteria and present our new method based on the magnitude of the order parameters. We also discuss the effect of the repulsive interaction in the PNJL phase diagrams obtained from our method. The change of a specific parameter in the Polyakov potential of the PNJL model is analyzed in this section, as well as the entanglement PNJL (EPNJL) model. Finally, in Sec. IV we present a summary and our main conclusions.

II. PNJL MODEL

The connection between the fermion (q) and the gauge (A^μ) field in the PNJL model is achieved by making the substitution $\partial^\mu \longrightarrow D^\mu = \partial^\mu - iA^\mu$ in the Lagrangian density, where $A^\mu = \delta^\mu_0 A_0$ and $A_0 = gA^0_\alpha \frac{\lambda_\alpha}{2}$ (g is the gauge coupling and λ_α are the Gell-Mann matrices). Techniques from field theory at finite temperature, as those used in Ref. [19], are applied to get the following grand canonical potential per volume:

$$\Omega_{\rm PNJL} = \mathcal{U}(\Phi, \Phi^*, T) + G_s\rho_s^2 - \frac{\gamma}{2\pi^2}\int_0^\Lambda Ek^2dk - \frac{\gamma}{6\pi^2}\int_0^\infty \frac{k^4}{E}dk[F(E,T,\mu_q,\Phi,\Phi^*) + \bar{F}(E,T,\mu_q,\Phi,\Phi^*)], \quad (1)$$

where $E = E(M) = (k^2 + M^2)^{1/2}$, ρ_s is the quark condensate given by $\rho_s = \langle\bar{q}q\rangle = \langle\bar{u}u\rangle + \langle\bar{d}d\rangle = 2\langle\bar{u}u\rangle$ in the isospin symmetric system, and $\gamma = N_s \times N_f \times N_c = 12$ is the degeneracy factor due to the spin ($N_s = 2$), flavor ($N_f = 2$), and color numbers ($N_c = 3$). The constituent quark mass is $M = m_0 - 2G_s\rho_s$. The second integral in Eq. (1) leads to the expected Stefan-Boltzmann limit, since the momentum of the active quarks are unconstrained.

The traced Polyakov loop is defined in terms of $A_4 = iA_0 \equiv T\phi$ as

$$\Phi = \frac{1}{3}\mathrm{Tr}\left[\exp\left(\mathrm{i}\int_0^{1/\mathrm{T}} \mathrm{d}\tau \mathrm{A}_4\right)\right] = \frac{1}{3}\mathrm{Tr}[\exp(\mathrm{i}\phi)] = \frac{1}{3}\mathrm{Tr}\{\exp[\mathrm{i}(\phi_3\lambda_3 + \phi_8\lambda_8)]\} = \frac{1}{3}[\mathrm{e}^{\mathrm{i}(\phi_3+\phi_8/\sqrt{3})} + \mathrm{e}^{\mathrm{i}(-\phi_3+\phi_8/\sqrt{3})} + \mathrm{e}^{-2i\phi_8/\sqrt{3}}] \quad (2)$$

in a gauge (Polyakov gauge) in which the gluon field is written in terms of the diagonal Gell-Mann matrices as $\phi = \phi_3\lambda_3 + \phi_8\lambda_8$, with ϕ_3, $\phi_8 \in \mathbb{R}$. Here, the definitions $\phi_3 = A_4^3/T$ and $\phi_8 = A_4^8/T$ were taken into account. It is worth mentioning that Φ^* is the complex conjugate of the complex field Φ.

As pointed out in Refs. [22,23], an important consequence of the coupling between Φ and the quark sector is the possibility to deal with the PNJL model in the same theoretical way as in the NJL one, regarding the statistical treatment. However, in this case new distribution functions for quarks and antiquarks appear and are given by

$$F(E,T,\mu_q,\Phi,\Phi^*) = \frac{\Phi e^{2(E-\mu_q)/T} + 2\Phi^* e^{(E-\mu_q)/T} + 1}{3\Phi e^{2(E-\mu_q)/T} + 3\Phi^* e^{(E-\mu_q)/T} + e^{3(E-\mu_q)/T} + 1}, \quad (3)$$

and $\bar{F}(E,T,\mu_q,\Phi,\Phi^*) = F(E,T,-\mu_q,\Phi^*,\Phi)$ generalized from the usual Fermi-Dirac distributions by the inclusion of Φ and Φ^*. Another difference in the PNJL model is the Polyakov loop potential $\mathcal{U}(\Phi,\Phi^*,T)$. Some versions of this potential were proposed in the literature, and following the language of Ref. [25], we refer to two of them by RTW05 [18] and RRW06 [19–24]. The other two are FUKU08 [25] and DS10 [48]. Their functional forms are given, respectively, by

$$\frac{\mathcal{U}_{\rm RTW05}}{T^4} = -\frac{b_2(T)}{2}\Phi\Phi^* - \frac{b_3}{6}(\Phi^3 + \Phi^{*3}) + \frac{b_4}{4}(\Phi\Phi^*)^2, \quad (4)$$

$$\frac{\mathcal{U}_{\rm RRW06}}{T^4} = -\frac{b_2(T)}{2}\Phi\Phi^* + b_4(T)\ln[h(\Phi,\Phi^*)], \quad (5)$$

$$\frac{\mathcal{U}_{\rm FUKU08}}{bT} = -54e^{-a/T}\Phi\Phi^* + \ln[h(\Phi,\Phi^*)], \quad (6)$$

$$\mathcal{U}_{\rm DS10} = (a_0T^4 + a_1\mu_q^4 + a_2T^2\mu_q^2)\Phi^2 + a_3T_0^4\ln[h(\Phi,\Phi)], \quad (7)$$

where

$$b_2(T) = a_0 + a_1\left(\frac{T_0}{T}\right) + a_2\left(\frac{T_0}{T}\right)^2 + a_3\left(\frac{T_0}{T}\right)^3, \quad (8)$$

$$h(\Phi,\Phi^*) = 1 - 6\Phi\Phi^* + 4(\Phi^3 + \Phi^{*3}) - 3(\Phi\Phi^*)^2, \quad (9)$$

and $b_4(T) = b_4(T_0/T)^3$. The constants of these parametrizations are given in Table I.

In a general way, the Polyakov potentials are constructed in order to reproduce the well-established data from lattice calculations of the pure gluon sector (where $\Phi = \Phi^*$) concerning the temperature dependence of the Polyakov loop and its first order phase transition characterized by the jump of Φ from the vanishing to a finite value at

TABLE I. Dimensionless parameters of the potentials given in Eqs. (4), (5), and (7). The constants of the FUKU08 potential are given by $a = 664$ MeV and $b = 0.03\Lambda^3$ MeV^3.

Potentials	a_0	a_1	a_2	a_3	b_3	b_4
RTW05	6.75	−1.95	2.625	−7.44	0.75	7.5
RRW06	3.51	−2.47	15.22	…	…	−1.75
DS10	−1.85	-1.44×10^{-3}	−0.08	−0.40	…	…

$T_0 = 270$ MeV (see the dotted curve of Fig. 2 in Ref. [19], for instance).

The free parameters $\Lambda = 651$ MeV, $m_0 = 5.5$ MeV, and $G_s = 5.04$ GeV^{-2}, are obtained from the NJL sector of the PNJL model in order to reproduce the vacuum values of $m_\pi = 140.51$ MeV, $f_\pi = 94.04$ MeV, and $|\langle\bar{u}u\rangle|^{1/3} = 251.32$ MeV for the pion mass, the pion decay constant, and the quark condensate, respectively.

To completely define the model, and consequently construct its phase diagram, one needs to evaluate the order parameters. This is done by requiring that $\Omega_{\rm PNJL}$ is minimized with respect to the set of fields of the model, i.e., ρ_s, ϕ_3, ϕ_8, or, equivalently, ρ_s, Φ, Φ^*. Therefore, the condition

$$\frac{\partial\Omega_{\rm PNJL}}{\partial X_i} = 0 \tag{10}$$

with $X_i = \rho_s, \phi_3, \phi_8$ or $X_i = \rho_s, \Phi, \Phi^*$ has to be satisfied. However, as pointed out in Ref. [49] in the context of the Polyakov-quark-meson model, Eq. (10) is only a necessary but not a sufficient condition to ensure that the values of X_i minimize $\Omega_{\rm PNJL}$. The authors discuss two distinct situations in which $\Omega_{\rm PNJL}$ presents no minima. The first of them is related to the fact that $\Omega_{\rm PNJL}$ is in general a complex-valued function due to the complex fields Φ and Φ^*. In this case, the minimum cannot be defined. One way to circumvent this problem very often used in the literature is to make $\Omega_{\rm PNJL}$ a real function by requiring that Φ and Φ^* be real and independent quantities. However, this assumption itself is not sufficient to ensure that the conditions (10) provide a field configuration which minimizes $\Omega_{\rm PNJL}$.

The authors of Ref. [49] show that some Polyakov potentials, such as RTW05 and RRW06 given, respectively, in Eqs. (4) and (5), are unbounded from below for some values of the real quantities Φ and Φ^*. For instance, it was shown that for $\Phi^* \to \infty$ and $\Phi = 0$, one has $\mathcal{U}_{\rm RTW05}, \mathcal{U}_{\rm RRW06} \to -\infty$. Therefore, there are no minima for $\Omega_{\rm PNJL}$ in such cases, even with $\Omega_{\rm PNJL}$ being a real function. In order to ensure that the real fields minimize $\Omega_{\rm PNJL}$, the authors suggest the use of condition (10) with the additional positivity constraint of all eigenvalues of the respective $i \times i$ Hessian matrix. The use of Eq. (10) without additional constraints to find the mean fields of the model is called the saddle point approach, frequently used in literature.

In our work, we will use the mean-field approximation described in Refs. [20,21] that takes into account the mean-field configuration in which $\phi_8 = 0$ in Eq. (2). In this case, $\Phi = \Phi^* = [2\cos(\phi_3) + 1]/3$ even for $\mu_q > 0$, which leads to $\Omega_{\rm PNJL} \in \mathbb{R}$. Another feature of this approach is that we do not have the problem of $\mathcal{U}_{\rm RTW05}, \mathcal{U}_{\rm RRW06} \to -\infty$, previously raised.

The condition given in Eq. (10), namely,

$$\frac{\partial\Omega_{\rm PNJL}}{\partial\rho_s} = \frac{\partial\Omega_{\rm PNJL}}{\partial\Phi} = 0, \tag{11}$$

generates the following set of coupled equations to be solved:

$$M - m_0 + 2G_s\rho_s[M, E(M), T, \mu_q, \Phi] = 0, \tag{12}$$

and

$$\frac{\partial\mathcal{U}(\Phi, T)}{\partial\Phi} - \frac{3T\gamma}{2\pi^2 N_c}\int_0^\infty k^2 dk[g(E(M), T, \mu_q, \Phi) + g(E(M), T, -\mu_q, \Phi)] = 0, \tag{13}$$

where the function $g(E, T, \mu_q, \Phi)$ leads to

$$g(E, T, \mu_q, \Phi) = \frac{1 + e^{-(E-\mu_q)/T}}{3\Phi[1 + e^{-(E-\mu_q)/T}] + e^{(E-\mu_q)/T} + e^{-2(E-\mu_q)/T}}. \tag{14}$$

The quark condensate is given by

$$\rho_s = \frac{\gamma M}{2\pi^2}\int_0^\infty \frac{k^2}{E} dk[F(E, T, \mu_q, \Phi) + \bar{F}(E, T, \mu_q, \Phi)] - \frac{\gamma M}{2\pi^2}\int_0^\Lambda \frac{k^2}{E(M)} dk. \tag{15}$$

Our study is based on the aforementioned saddle point approach. In addition, in the case of the mean-field approximation used here ($\phi_8 = 0$), we have also checked the sign of the Hessian matrix eigenvalues. In general, our solutions correspond to minima of $\Omega_{\rm PNJL}$. Negative eigenvalues were found only for a small region of T and μ_q around the first order phase transition. Nevertheless, the projection of the order parameters in the $T \times \mu_q$ plane from the saddle point approach that we will present in the next section does not differ significantly from the one obtained by the method proposed in Ref. [49]. Our calculations confirm the findings of Ref. [49], that the phase boundary is not changed by considering the saddle point approach for the RRW06 potential adopted in our work.

It is worth noting that in such equations, we still did not consider the repulsive interaction, which has its magnitude given by the coupling constant G_V. The impact of this specific interaction in the phase diagrams will be analyzed in Sec. III B, and in these cases, the saddle point solutions provide minima of $\Omega_{\rm PNJL}$.

III. RESULTS AND DISCUSSION

A. Phase diagrams without vector interaction

For each pair (T, μ_q), the Eqs. (11) and (13) are solved for the quantities M and the Polyakov loop that are used in Eq. (15) in order to evaluate the quark condensate. In this way, one has for the given pair (T, μ_q) both order parameters, ρ_s and Φ, basic thermodynamical quantities used to construct the quark phase diagram. Frequently, many authors use the criterion of finding the maxima of $\partial\rho_s/\partial T$ and $\partial\Phi/\partial T$ to generate the $T \times \mu_q$ diagram. Thus, from this assumption, one can obtain the following behavior depicted in Fig. 1 constructed for the RRW06 parametrization at vanishing chemical potential.

This behavior indicates a smooth crossover instead of a first order phase transition. Therefore, the transition temperature (or the pseudocritical temperature, as it is also named) is defined as that in which a maximum is found. In the case of $\mu_q = 0$, the maxima of $\partial\rho_s/\partial T$ and $\partial\Phi/\partial T$ occur practically at the same temperature, $T \sim 220$ MeV. Thus, the corresponding point in the $T \times \mu_q$ plane for this case is $\mu_q = 0$, $T \sim 220$ MeV.

The peak structure of $\partial\Phi/\partial T$ exhibited in Fig. 2(a) does not keep the same as in Fig. 1 for higher chemical potential values. Notice that from a determined chemical potential value, a multiple extrema structure takes place in $\partial\Phi/\partial T$, different from the $\partial\rho_s/\partial T$ case, that presents only one maximum for any chemical potential, see Fig. 2(b). For those $\partial\Phi/\partial T$ curves in which this effect is exhibited, the first peaks always coincide with those in the $\partial\rho_s/\partial T$ curve at the same μ_q. The reason can be understood from the coupling between Eqs. (12) and (13). The peak in $\partial\Phi/\partial T$ coming from the abrupt fall in the quark condensate is reflected in the Polyakov loop via Eq. (13), since $E = \sqrt{k^2 + (m_0 - 2G_s\rho_s)^2}$. This variation in ρ_s influences Φ also generating an abrupt change in its value and, consequently, a peak in $\partial\Phi/\partial T$. The second peak is uniquely

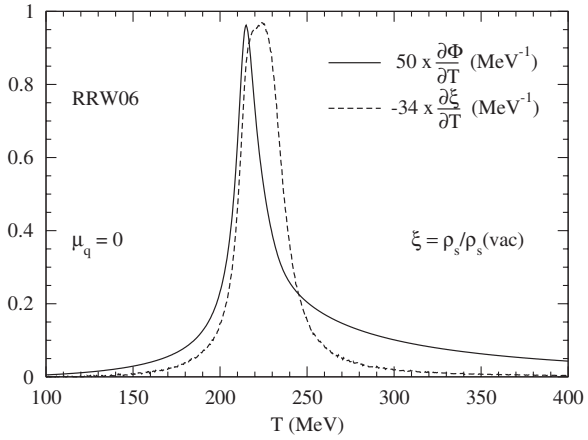

FIG. 1. Temperature derivatives of the order parameters as a function of T for the RRW06 parametrization at $\mu_q = 0$.

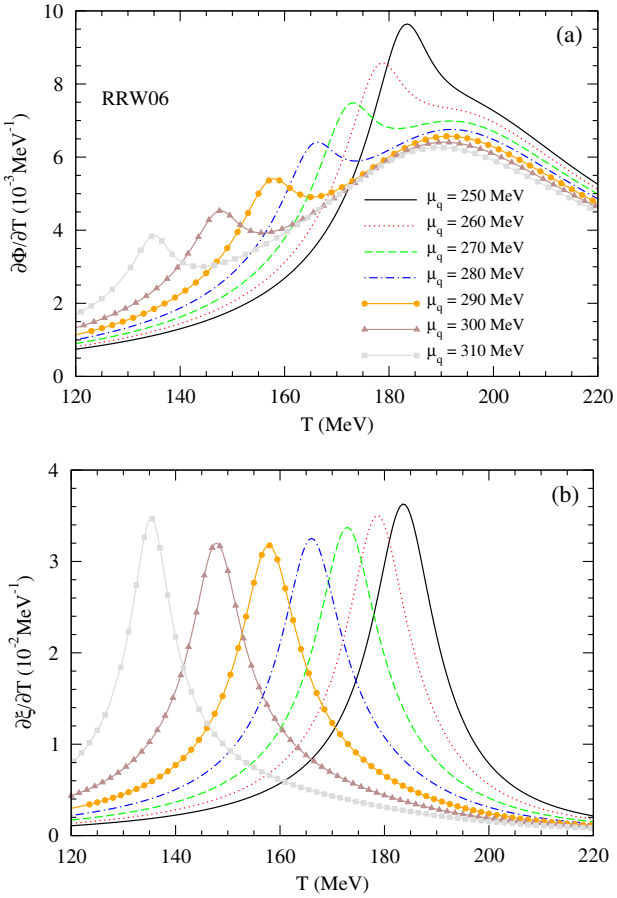

FIG. 2 (color online). Temperature derivatives of (a) Φ and (b) $\xi = \rho_s/\rho_{s(\mathrm{vac})}$, as a function of T at finite μ_q values.

coming from the Polyakov loop dynamics itself since in this temperature range, the quark condensate practically vanishes. This possibility of more than one peak in the temperature derivatives of the order parameters was already reported for the PNJL model [36], as well as in the linear sigma model coupled with the Polyakov loop [36–38].

We point out here that the construction of the phase diagram based on the choice of the coincident peaks in $\partial\rho_s/\partial T$ and $\partial\Phi/\partial T$ leads to a situation where the region in which the chiral symmetry is broken (restored) and that one in which the quarks are confined (deconfined) are exactly the same. Therefore, there is no possibility to identify, following this criterion, a quarkyonic phase [50] region where the chiral symmetry is restored but with quarks still confined.

Another criterion used to construct the PNJL diagrams is to investigate the magnitude of the order parameters, since their values are directly related to the symmetries that are broken or are not in the regions delimited by the boundary curves in the $T \times \mu_q$ plane. It is well known that $\rho_s \neq 0$ indicates broken chiral symmetry, and $\rho_s = 0$ means that this symmetry is restored. The same concept is adopted for the Polyakov loop Φ. The difference is that the involved symmetry is the center symmetry, closely associated with

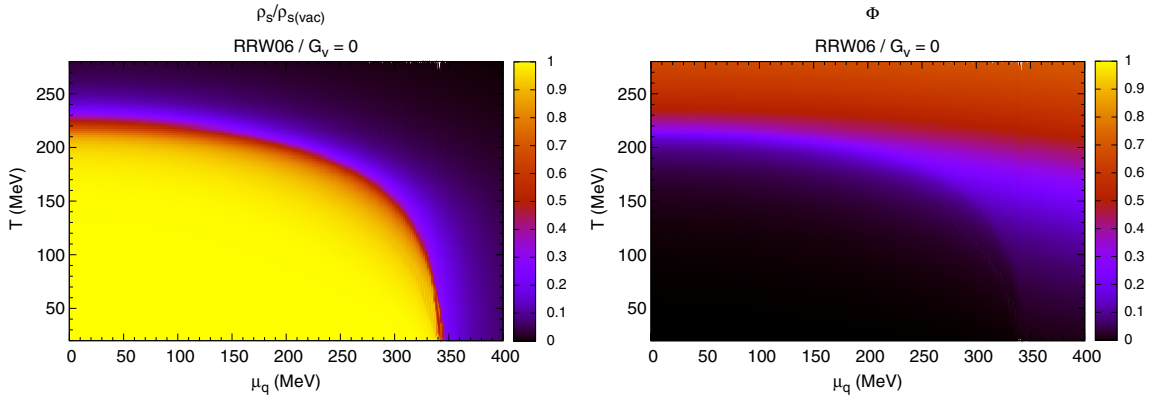

FIG. 3 (color online). Order parameters' surfaces ρ_s (left panel) and Φ (right panel) projected in the $T \times \mu_q$ plane.

the confinement phenomenon [51]. In this case, the pseudocritical temperature is defined by Fukushima [25] as that in which all the order parameters normalized by its vacuum values (with exception for the Polyakov loop) reach the value of $1/2$. Thus, the author constructed three distinct boundary curves, also identifying the quarkyonic phase, in this case for the SU(3) version of the PNJL model, see Fig. 12 of Ref. [25].

Our purpose here is to furnish an alternative and more natural criterion to identify the different quark phases and their boundary curves while also using the magnitude of ρ_s and Φ. The method is based on the analysis of the projected surface of the order parameters as a function of T and μ_q. An example is given in Fig. 3 for the RRW06 parametrization.

The broken and restored chiral symmetry regions are very well defined, as well as their boundaries in the left panel. In the Φ plot (right panel), one can also recognize the confined and deconfined quark phases. The interesting feature in this diagram is the natural emergence of a phase between the confined and the deconfined one. To become clear that such a phase is the quakyonic one, we plot inside these diagrams the curves delimiting all regions. The result is shown in Fig. 4.

The lower full curves were generated by making fixed the value of $\rho_s/\rho_{s(\mathrm{vac})}$. From Fig. 3, the color code suggests that the $1/2$ value is a good representative of the boundary between the broken and restored chiral symmetry phases. In the case of the Polyakov loop curves, upper full ones, we found $\Phi = 0.4$ as a reasonable value to delimit the onset of the deconfined quark phase. We remark here that other values could represent this boundary line, depending on the used model. The authors of Ref. [24] (see their Figs. 1 and 5) used a value of $\Phi = 0.3$ for the nonlocal version of the PNJL model in the chiral limit and for finite quark masses but using a Landau expansion and susceptibilities to find the crossover chiral line. Also, Fukushima defined $\rho_s/\rho_{s(\mathrm{vac})} = \Phi = 1/2$ to represent the $\rho_s/\rho_{s(\mathrm{vac})}$ and Φ boundaries in the PNJL-SU(3) model [25], claiming that the magnitude of the order parameter was a more suitable quantity to probe the physical state of matter. Here, we construct the boundary lines by finding the suitable values of the order parameters from their projection on the $T \times \mu_q$ plane.

From Fig. 4 is clear that the region between the two full lines is the quarkyonic phase exhibited in our calculations even in the SU(2) version of the PNJL parametrizations presented here. In the same figure, we also furnish the first

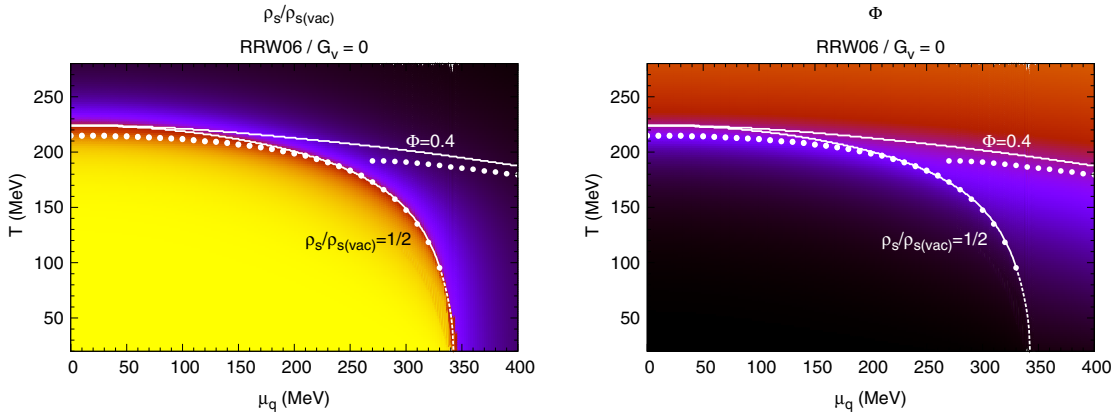

FIG. 4 (color online). The same as in Fig. 3. Full lines: curves corresponding to the points in which $\rho_s/\rho_{s(\mathrm{vac})} = 1/2$ and $\Phi = 0.4$. Full circle curves: obtained from the peaks in $\partial\rho_s/\partial T$ and $\partial\Phi/\partial T$. Dashed lines: first order phase transitions curves.

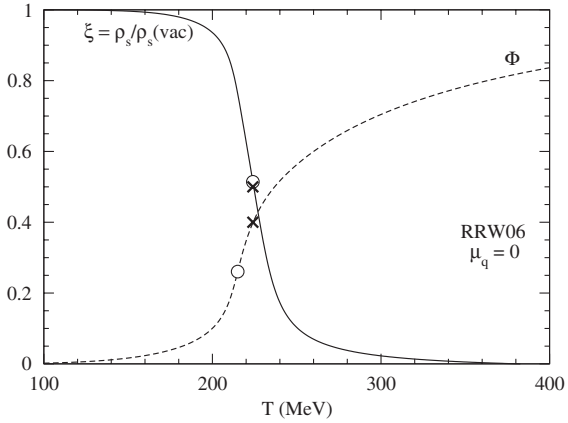

FIG. 5. Order parameters as a function of T. Circles: peaks' positions of $\partial\Phi/\partial T$ and $\partial\rho_s/\partial T$. Crosses: points' positions of $\Phi = 0.4$ and $\rho_s/\rho_{s(\mathrm{vac})} = 1/2$.

order transition lines (dashed ones). In order to clarify the definition of the solid boundaries in Fig. 4, we present in Fig. 5 the temperature dependence of the order parameters for $\mu_q = 0$. In this figure, we show by the circles the peaks' positions of $\partial\Phi/\partial T$ and $\partial\rho_s/\partial T$. The position of the points in which $\Phi = 0.4$ and $\rho_s/\rho_{s(\mathrm{vac})} = 1/2$ are denoted by the crosses.

In order to compare this new method of construction of the boundary lines with those that use the peaks criterion, we also display in Fig. 4 the points corresponding to the peaks of $\partial\rho_s/\partial T$ and $\partial\Phi/\partial T$. In the range of $0 < \mu_q \lesssim 270$ MeV, the derivative curves present only one peak that is almost coincident, see Fig. 2. Therefore, it is possible to determine only one curve in the $T \times \mu_q$ plane (circles starting at $\mu_q = 0$ in Fig. 4). From $\mu_q \sim 270$ MeV, the $\partial\Phi/\partial T$ curve presents two peaks, one of them, the first one, the same as in the $\partial\rho_s/\partial T$ curve. The second peaks of $\partial\Phi/\partial T$ are represented in Fig. 4 by the circles starting at $\mu_q \sim 270$ MeV. The composition of the first and second peaks' lines leads to delimit a smaller quarkyonic phase when we compare it to that obtained by the region between the two full lines. This feature is also verified when we add an additional vector interaction in the PNJL model.

In the cases in which one chooses only the first peaks in the $\partial\Phi/\partial T$ curve, the circles starting at $\mu_q \sim 270$ MeV would not appear, and consequently, there would be no quarkyonic phase. In this case, the quark phase diagram would lose essential information. This does not happen if we use the method of the magnitude of the order parameters to construct the boundary curves. The quarkyonic phase is always present in the phase diagram.

We have checked that by using $\Phi \neq \Phi^*$, the phase diagrams are not altered significantly. We illustrate our computation in Fig. 6 for the potential RRW06, which should be compared with Fig. 3. We present results of the phase diagrams for ρ_s, Φ, and Φ^*. We observe negligible differences in the Φ and Φ^* projections compared to the Φ

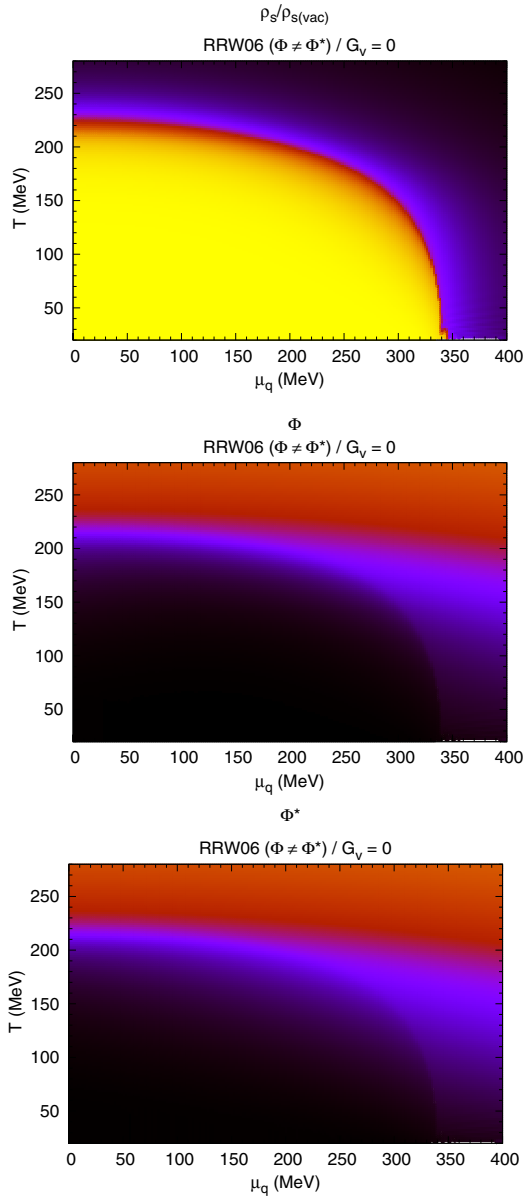

FIG. 6 (color online). Order parameters' surfaces for ρ_s (upper panel), Φ (middle panel), and Φ^* (lower panel) projected in the $T \times \mu_q$ plane.

one for the $\Phi = \Phi^*$ case shown in Fig. 3. The same pattern is verified in the case of ρ_s.

Our results corroborate the findings of Ref. [18] for a single μ_q value, giving support to the assumption $\Phi = \Phi^*$ used in our work for a large region of $\mu_q > 0$ and necessary for the study of PNJL phase diagrams.

B. Effect of the vector interaction

It is known that a vector-type interaction in the PNJL model is responsible for shrinking the first order phase transition [25,52,53]. Therefore, the critical end point is moved in the direction to be completely removed, as the strength of the interaction is increasing. The same effect

could also be observed in the NJL model [11,54]. The inclusion of a vector term of the form $-G_V(\bar{q}\gamma^\mu q)^2$ in the PNJL Lagrangian density modifies the grand canonical potential as

$$\Omega_{\mathrm{PNJL}}(\mu_q, T, \Phi) \rightarrow \Omega_{\mathrm{PNJL}}(\tilde{\mu_q}, T, \Phi) - G_V\rho^2, \qquad (16)$$

with

$$\tilde{\mu_q} = \mu_q - 2G_V\rho \qquad (17)$$

being the effective chemical potential and ρ the quark density. All the other quantities and equations are modified by making $\mu_q \rightarrow \tilde{\mu_q}$. Therefore, besides Eqs. (12) and (13), Eq. (17) should be taken into account also in the self-consistent solutions of the order parameters.

Other effect of the vector interaction is to change the double peak structure in $\partial\Phi/\partial T$ compared to the case in which $G_V = 0$. Figure 7 shows this behavior for the $G_V = 0.2G_s$ case. Notice that in this case, there is only one peak. The boundary curve constructed from the analysis of $\partial\Phi/\partial T$ is shown in the Φ projected curve in the $T \times \mu_q$ plane of Fig. 8. In the same figure, we also show the boundary lines constructed by taking the fixed values of $\rho_s/\rho_{s(\mathrm{vac})} = 1/2$ and $\Phi = 0.4$.

It is clear that if the peak's criterion in $\partial\Phi/\partial T$ is adopted in this situation, the obtained curve is not sufficient to correctly delimit all the possible phases of the system, as in the case of $G_V = 0$, see Fig. 4. Therefore, it is also necessary to use the peaks of $\partial\rho_s/\partial T$ to make clear the distinct regions. Notice also the difference between the curve obtained via the $\partial\Phi/\partial T$ peaks and that constructed via $\Phi = 0.4$. The latter one is more precise in the description of the boundary of the confinement/deconfinement phases.

Finally, we show how the strength of the vector interaction affects the quarkyonic phase in the PNJL model. Figure 9 shows the behavior of the order parameters for some values of G_V. The pattern exhibited shows that the

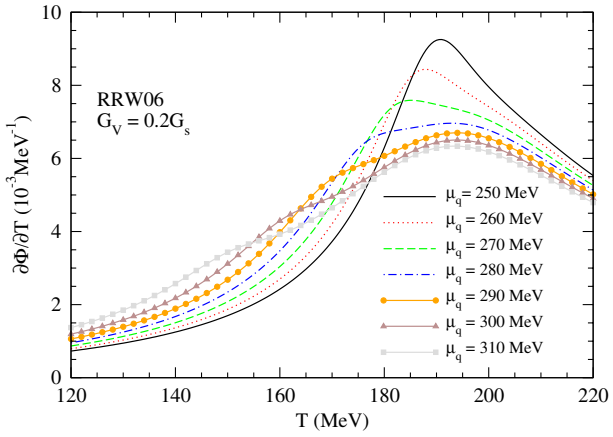

FIG. 7 (color online). Temperature derivative of the order parameter Φ as a function of the temperature for $G_V = 0.2G_s$.

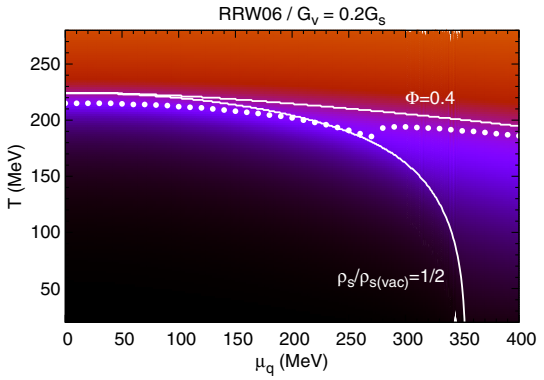

FIG. 8 (color online). Φ projection at the $T \times \mu_q$ plane for $G_V = 0.2G_s$.

quarkyonic phase tends to become smaller as G_V is increased.

Even with such bands shown when G_V is increased, it is still possible to use the magnitude of the order parameters to define boundaries of the broken/restored chiral symmetry and confinement/deconfinement phases. Indeed, we have studied in Ref. [40] the quark phase diagrams of PNJL models constructing the boundary of the broken/restored chiral symmetry phase, for distinct G_V values, using different values of $\rho_s/\rho_{s(\mathrm{vac})}$. Notice also a diffusing effect on the values of ρ_s, mainly at higher values of μ_q. A similar behavior is also verified for different values of the T_0 parameter in the PNJL models even at $G_V = 0$. In next

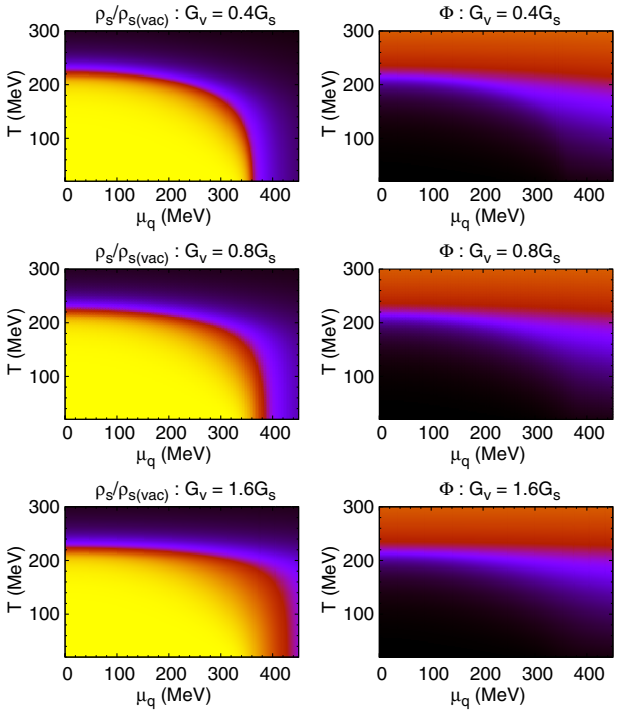

FIG. 9 (color online). Projection of the order parameter surfaces ρ_s (left panels) and Φ (right panels) in the $T \times \mu_q$ plane for different G_V values in the RRW06 potential.

subsection, we show the case for $T_0 = 205$ MeV in the RRW06 parametrization.

Notice also that the effect of moving the boundary related to the broken/restored chiral symmetry phases is not observed in the Φ projection. In this case, the boundary of the confined/deconfined phases remains unchanged. The quarkyonic phase is moved to the direction of increasing μ_q values, but the phase related to free massless quarks is unaffected.

As a last remark of the inclusion of the vector interaction, we point out that the projections of the order parameters generated by the saddle point approach and by the method of Ref. [49] are exactly the same, since for the values of G_V used here, there are no regions of first order phase transitions, and therefore, no regions of negative eigenvalues of the Hessian matrix.

C. Effect of the T_0 parameter and the EPNJL model

The Polyakov potentials presented in Eqs. (3)–(5) have their free parameters adjusted to correctly reproduce some lattice QCD results for the pure gluon sector (quenched approximation). In particular, the value of $T_0 = 270$ MeV is the temperature in which the gluonic system presents a first order phase transition. The discontinuity in this case is verified in the Polyakov loop plotted as a function of T. With the found parameters, the PNJL model is used to describe, in an effective way, the system with quarks and gluons. However, the transition temperature found in the PNJL models at $\mu_q = 0$ is higher than that obtained by lattice QCD calculations. The latter is given by 173 ± 8 MeV [55]. The former is calculated as $T(\mu_q = 0) > 200$ MeV through the peak's criterion or even using the magnitude of the order parameters (projection in the $T \times \mu_q$), see the starting point at $\mu_q = 0$ of the circles and full curves in Fig. 4.

In order to make the PNJL model consistent with the lattice results at $\mu_q = 0$, the rescaling in T_0 is often used in the literature. The change to $T_0 = 190$ MeV decreases the transition temperature of the PNJL models at zero chemical potential to compatible values when the peak's criterion is adopted. However, as pointed out in Ref. [18], the peaks of $\partial\rho_s/\partial T$ and $\partial\Phi/\partial T$ are not coincident anymore, as in the case in which $T_0 = 270$ MeV. Due to lattice QCD, studies indicate that quark deconfinement and chiral restoration occurs at the same temperature at $\mu_q = 0$; this problem is circumvented in the PNJL model by taking the average temperatures associated to the peaks of $\partial\rho_s/\partial T$ and $\partial\Phi/\partial T$. Such a procedure generates only one boundary curve in the $T \times \mu_q$ plane, characterizing one region in which (i) chiral symmetry is broken with confined quarks, and (ii) the other one presenting restoration of chiral symmetry and deconfined quarks. There is no possibility of a quarkyonic phase (restored chiral symmetry and confined quarks). This is not the case if we construct the boundary curves from the analysis of the ρ_s and Φ projections, as we will make clear below.

If the projection of the order parameters in the $T \times \mu_q$ plane is used, it is also possible find suitable values of the transition temperature in the PNJL model at $\mu_q = 0$. This is done in Fig. 10 by rescaling T_0 from 270 to 205 MeV.

Important points regarding the phase diagrams exhibited in this figure deserve to be discussed. First of all, notice that the change in the T_0 parameter makes the boundary of the broken/restored chiral symmetry phases larger than that presented in Fig. 3. The "red line" in Fig. 3 gives rise to the "red band" in Fig. 10. It means that if we want to construct a boundary curve in the $T \times \mu_q$ plane, it has to be inside such a band. The same does not occur for the Φ projection. Notice that we still can define unambiguously a curve separating the confined and deconfined phases. Indeed, such a curve is constructed by making $\Phi = 0.44$, a value that furnishes a curve in which the transition temperature at $\mu_q = 0$ is compatible with lattice QCD results. Since this curve is defined, one has to find a fixed value of $\rho_s/\rho_{s(\mathrm{vac})}$ in order to make the boundary curve of the broken/restored chiral symmetry phases present the same transition temperature at $\mu_q = 0$. The value found in this case was $\rho_s/\rho_{s(\mathrm{vac})} = 0.77$.

The choice of $\rho_s/\rho_{s(\mathrm{vac})} = 0.77$ is not unique. Different values that make the boundary curve inside the red band

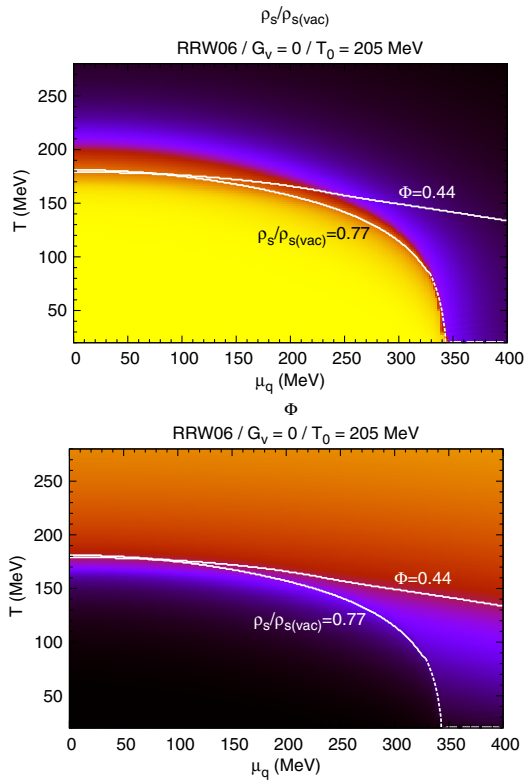

FIG. 10 (color online). ρ_s (upper panel) and Φ (lower panel) surfaces projected in the $T \times \mu_q$ plane for RRW06 parametrization with $T_0 = 205$ MeV.

can be found. However, these values generate curves that do not have the same transition temperature at $\mu_q = 0$ as that presented by the $\Phi = 0.44$ curve. Moreover, such temperatures are different from approximately 170 MeV. Therefore, they do not satisfy the constraint established by the lattice results.

An important aspect shows in Fig. 10 that the change in the T_0 parameter makes the confined phase smaller than that presented in the case in which T_0 has its original value of 270 MeV. Actually, this is the reason why the transition temperature at $\mu_q = 0$ is compatible with the lattice results. The same is not verified for the broken chiral symmetry phase. The change in the values of Φ induced by the T_0 rescaling is not totally followed by ρ_s. As already mentioned, the boundary of the phases in the ρ_s projection on the $T \times \mu_q$ plane becomes a band that is still larger for lower values of T_0. This is due to the "weak interaction" between the order parameters Φ and ρ_s presented in the structure of the PNJL models treated here. This shortcoming in the PNJL models can be circumvented by including a Φ dependence in the scalar coupling G_s, i.e., by making $G_s = G_s(\Phi)$. In order to illustrate the effect of such a modification, we use the Φ dependence on G_s as given by

$$G_s(\Phi) = G_s[1 - \alpha_1 \Phi\Phi^* - \alpha_2(\Phi^3 + \Phi^{*3})], \qquad (18)$$

closely following Ref. [56], even concerning the values of $\alpha_1 = \alpha_2 = 0.2$. The PNJL model modified by making $G_s \rightarrow G_s(\Phi)$ is named the EPNJL model [57], since $G_s = G_s(\Phi)$ is an effective vertex called an entanglement vertex [56]. In Fig. 11, we show the order parameters' projections of the RRW06 parametrization of the EPNJL model for $T_0 = 200$ MeV.

Notice that the consequence of the strong correlation between ρ_s and Φ in the phase diagrams of the EPNJL model is to reduce the red band to a line in the ρ_s projection. In this case, the boundary line of the broken/restored chiral symmetry phases is unambiguously given by $\rho_s/\rho_{s(\mathrm{vac})} = 1/2$, exactly as in the case of the PNJL model for $T_0 = 270$ MeV, see Fig. 4. Also, the boundary curve of the confined/deconfined is defined by fixing the value of $\Phi = 0.4$. Now, both curves start at a transition temperature at $\mu_q = 0$ comparable to the lattice result of 173 ± 8 MeV.

Another important result shown in Fig. 11 is that the information on the quarkyonic phase is never lost. The full boundary curves constructed by defining $\rho_s/\rho_{s(\mathrm{vac})} = 1/2$ and $\Phi = 0.4$ always delimit a phase where the chiral symmetry is restored and the quarks are still confined. Therefore, it is possible also to represent all the phases and boundaries of strongly matter with the EPNJL model. Moreover, notice also that the EPNJL model provides the emergence of the quarkyonic phase only from $\mu_q \sim 240$ MeV for $G_V = 0$ differently for the case of the PNJL model of Fig. 10, where the quarkyonic phase starts at $\mu_q \sim 130$ MeV.

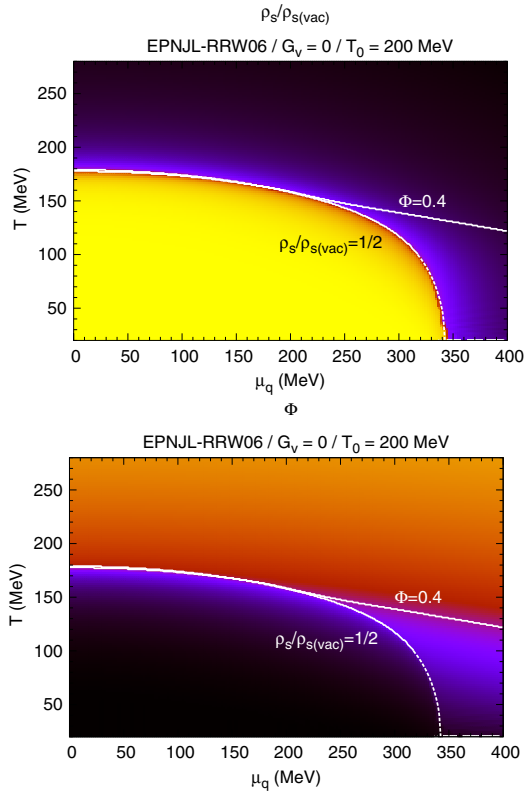

FIG. 11 (color online). ρ_s (upper panel) and Φ (lower panel) surfaces of the EPNJL model projected in the $T \times \mu_q$ plane for the RRW06 parametrization with $T_0 = 200$ MeV.

Finally, we stress here that our method of construction of the quark phase diagrams with all possible boundaries making the projections of ρ_s and Φ suggests that the order parameters should be more correlated to each other in order to unambiguously define the boundaries from the magnitude of ρ_s and Φ. As our results point out, the EPNJL model that presents such a correlation at any temperature and chemical potential seems to be a better candidate to describe the strongly interacting matter phase diagrams than the PNJL model itself. This result corroborates the lattice QCD calculation that points to this correlation at $\mu_q = 0$, since it obtains the same temperature transition related to both order parameters, namely, $T(\mu_q = 0) = 173 \pm 8$ MeV.

IV. SUMMARY AND CONCLUSIONS

In this work, we have proposed a method of identifying the phases and boundaries of strongly interacting matter obtained through the PNJL model. This method consists of analyzing the magnitude of the order parameters ρ_s and Φ by projecting their surfaces in the $T \times \mu_q$ plane. Therefore, it is natural to localize the broken/restored chiral symmetry and confinement/deconfinement phases, see an example of such a projection for the RRW06 parametrization in Fig. 3. The projections also allow the

determination of a particular value of $\rho_s/\rho_{s(\mathrm{vac})}$ and Φ used to construct the boundaries in the phase diagram. In the case of the RRW06 model, the boundary curves are defined as those in which $\rho_s/\rho_{s(\mathrm{vac})} = 1/2$ and $\Phi = 0.4$ are represented by the full curves in Fig. 4. We also compared our boundary curves with those determined through the peaks of $\partial\rho_s/\partial T$ and $\partial\Phi/\partial T$, frequently used in the literature and showed that the quarkyonic phase found by the latter is underestimated when compared to that found by the former.

The vector repulsive interaction in the PNJL model was other important aspect studied in our work. We have shown that is not possible to construct two boundaries in the phase diagram if only peaks of $\partial\Phi/\partial T$ are taken into account. The double peak structure of $\partial\Phi/\partial T$ in Fig. 2(a) is changed to the one depicted in Fig. 7. By using the fixed values of the order parameters from the aforementioned projections, it is natural to define the boundary curves even for the $G_V > 0$ cases. It is also clear that the increase of G_V decreases the quarkyonic phase, see Fig. 9.

Finally, we have investigated the influence of the T_0 parameter of the Polyakov potential RRW06 given in Eq. (5). If we keep the value of $T_0 = 270$ MeV in the original version of the RRW06 parametrization, the boundary curves constructed via the peak's criterion or by the magnitude of the order parameters (projection on $T \times \mu_q$ plane) give a value greater than 200 MeV for the transition temperature at $\mu_q = 0$, which is not supported by lattice QCD calculations that give the result of 173 ± 8 MeV. The common procedure adopted in the literature is the rescaling of T_0 from 270 to 190 MeV, taking the average values of the transition temperatures associated with the peaks of $\partial\rho_s/\partial T$ and $\partial\Phi/\partial T$ (not coincident for T_0 rescaled). This generates only one boundary curve and does not allow the emergence of a quarkyonic phase in the SU(2) version of the PNJL model. In our method based on the analysis of the projection of the order parameters, the suitable rescaling is to change T_0 from $T_0 = 270$ MeV to $T_0 = 205$ MeV. This is the value that allows us to construct the two boundary curves presented in Fig. 10 starting at the same point at $\mu_q = 0$ and presenting compatible values for the transition temperature. In this case, the curves have the values of 0.77 and 0.44 associated with $\rho_s/\rho_{s(\mathrm{vac})}$ and Φ, respectively. The region surrounded by the two curves is the quarkyonic phase.

We also concluded that the value of 0.77 is not unique to define a boundary curve of the broken/restored chiral symmetry phases for $T_0 = 205$ MeV. Such an ambiguity can be removed if the correlation between the order parameters is increased by making $G_s \rightarrow G_s(\Phi)$. The EPNJL model constructed in this way produces the projections of ρ_s and Φ obtained in Fig. 11. The boundary of the broken/restored chiral symmetry phases is again uniquely defined by the $\rho_s/\rho_{s(\mathrm{vac})} = 1/2$ curve and present a value of $T(\mu_q = 0) \sim 170$ MeV, compatible with the lattice result for this quantity. Also, the $\Phi = 0.4$ curve starts at the same point at $\mu_q = 0$. From this perspective, our results show that the EPNJL model describes in an unambiguous way all phases and boundaries of quark matter, better than the PNJL model. This indicates that the correlation between the order parameters of the quark phase transition must be strongly correlated, as the lattice QCD results for the temperature transition at $\mu_q = 0$ point out.

As a last remark, we stress here the importance and need of theoretical studies of the strongly interacting matter phase diagram, mainly in the region of higher chemical potentials (compressed matter), since this is a region where new experiments will focus in the near future, for instance, at the Facility for Antiproton and Ion Research (FAIR) [46] and at the Joint Institute for Nuclear Researches (JINR) [47].

ACKNOWLEDGMENTS

The authors acknowledge the partial support from Fundação de Amparo à Pesquisa do Estado de São Paulo (FAPESP) and Conselho Nacional de Desenvolvimento Científico e Tecnológico (CNPq) of Brazil.

[1] J. B. Kogut, Rev. Mod. Phys. **51**, 659 (1979); **55**, 775 (1983); H. J. Rothe, *Lattice Gauge Theories. An Introduction* (World Scientific, Singapore, 1997); P. Petreczky, J. Phys. G **39**, 093002 (2012).

[2] D. P. Landau and K. Binder, *A Guide to Monte Carlo Simulations in Statistical Physics* (Cambridge University Press, Cambridge, England, 2000).

[3] K. Splittorff and J. J. M. Verbaarschot, Phys. Rev. Lett. **98**, 031601 (2007).

[4] C. R. Allton, S. Ejiri, S. J. Hands, O. Kaczmarek, F. Karsch, E. Laermann, Ch. Schmidt, and L. Scorzato, Phys. Rev. D **66**, 074507 (2002); C. R. Allton, S. Ejiri, S. J. Hands, O. Kaczmarek, F. Karsch, E. Laermann, and C. Schmidt, Phys. Rev. D **68**, 014507 (2003); C. R. Allton, M. Döring, S. Ejiri, S. J. Hands, O. Kaczmarek, F. Karsch, E. Laermann, and K. Redlich, Phys. Rev. D **71**, 054508 (2005).

[5] Z. Fodor and S. D. Katz, Phys. Lett. B **534**, 87 (2002); J. High Energy Phys. 03 (2002) 014; Z. Fodor, S. D. Katz, and K. K. Szabo, Phys. Lett. B **568**, 73 (2003).

[6] E. Laermann and O. Philipsen, Annu. Rev. Nucl. Part. Sci. **53**, 163 (2003).

[7] P. de Forcrand and O. Philipsen, Nucl. Phys. **B642**, 290 (2002); **B673**, 170 (2003); M. D'Elia and M. P. Lombardo,

Phys. Rev. D **67**, 014505 (2003); **70**, 074509 (2004); M. D'Elia, F. Di Renzo, and M. P. Lombardo, Phys. Rev. D **76**, 114509 (2007).
[8] Z. Fodor, S. D. Katz, and C. Schmidt, J. High Energy Phys. 03 (2007) 121.
[9] A. Chodos, R. L. Jaffe, K. Johnson, C. B. Thorn, and V. F. Weisskopf, Phys. Rev. D **9**, 3471 (1974); A. Chodos, R. L. Jaffe, K. Johnson, and C. B. Thorn, Phys. Rev. D **10**, 2599 (1974); T. DeGrand, R. L. Jaffe, K. Johnson, and J. Kiskis, Phys. Rev. D **12**, 2060 (1975).
[10] Y. Nambu and G. Jona-Lasinio, Phys. Rev. **122**, 345 (1961); **124**, 246 (1961).
[11] M. Buballa, Phys. Rep. **407**, 205 (2005).
[12] U. Vogl and W. Weise, Prog. Part. Nucl. Phys. **27**, 195 (1991); S. P. Klevansky, Rev. Mod. Phys. **64**, 649 (1992); T. Hatsuda and T. Kunihiro, Phys. Rep. **247**, 221 (1994).
[13] K. Fukushima, Phys. Lett. B **591**, 277 (2004).
[14] E. Megías, E. R. Arriola, and L. L. Salcedo, Phys. Rev. Lett. **109**, 151601 (2012).
[15] A. Bhattacharyya, P. Deb, S. K. Ghosh, R. Ray, and S. Sur, Phys. Rev. D **87**, 054009 (2013); A. Bhattacharyya, S. K. Ghosh, S. Majumder, and R. Ray, Phys. Rev. D **86**, 096006 (2012).
[16] H. Kouno, T. Makiyama, T. Sasaki, Y. Sakai, and M. Yahiro, J. Phys. G **40**, 095003 (2013).
[17] R. Gatto and M. Ruggieri, Lect. Notes Phys. **871**, 87 (2013).
[18] C. Ratti, M. A. Thaler, and W. Weise, Phys. Rev. D **73**, 014019 (2006).
[19] C. Ratti, S. Rößner, M. A. Thaler, and W. Weise, Eur. Phys. J. C **49**, 213 (2007).
[20] S. Rößner, C. Ratti, and W. Weise, Phys. Rev. D **75**, 034007 (2007).
[21] S. Rößner, T. Hell, C. Ratti, and W. Weise, Nucl. Phys. **A814**, 118 (2008).
[22] H. Hansen, W. M. Alberico, A. Beraudo, A. Molinari, M. Nardi, and C. Ratti, Phys. Rev. D **75**, 065004 (2007).
[23] P. Costa, M. C. Ruivo, C. A. de Sousa, H. Hansen, and W. M. Alberico, Phys. Rev. D **79**, 116003 (2009).
[24] G. A. Contrera, M. Orsaria, and N. N. Scoccola, Phys. Rev. D **82**, 054026 (2010).
[25] K. Fukushima, Phys. Rev. D **77**, 114028 (2008).
[26] E. Blanquier, J. Phys. G **38**, 105003 (2011).
[27] L. M. Haas, R. Stiele, J. Braun, J. M. Pawlowski, and J. Schaffner-Bielich, Phys. Rev. D **87**, 076004 (2013).
[28] D. Blaschke, J. Berdermann, and R. Lastowiecki, Prog. Theor. Phys. Suppl. **186**, 81 (2010).
[29] K. Fukushima, J. Phys. Conf. Ser. **312**, 012001 (2011); K. Fukushima and T. Hatsuda, Rep. Prog. Phys. **74**, 014001 (2011); K. Fukushima and C. Sasaki, Prog. Part. Nucl. Phys. **72**, 99 (2013).
[30] P. K. Srivastava and C. P. Singh, Phys. Rev. D **85**, 114016 (2012); K. Masuda, T. Hatsuda, and T. Takatsuda, Astrophys. J. **764**, 12 (2013); G. Y. Shao, M. Colonna, M. Di Toro, Y. X. Liu, and B. Liu, Phys. Rev. D **87**, 096012 (2013); R. Cavagnoli, C. Providência, and D. P. Menezes, Phys. Rev. C **83**, 045201 (2011); T. Sasaki, N. Yasutake, M. Kohno, H. Kouno, and M. Yahiro, arXiv:1307.0681v2; N. Yasutake, T. Noda, H. Sotani, T. Maruyama, and T. Tatsumi (Nova Science Publishers, New York, 2013), Chap. 4.
[31] V. V. Begun, M. Gaździcki, and M. I. Gorenstein, Phys. Rev. C **88**, 024902 (2013); A. Tawfik and H. Magdy, arXiv:1206.0901v1.
[32] E. Megías, E. R. Arriola, and L. L. Salcedo, Nucl. Phys. B, Proc. Suppl. **234**, 313 (2013); V. Dexheimer, R. Negreiros, and S. Schramm, Eur. Phys. J. A **48**, 189 (2012); M. Hempel, V. Dexheimer, S. Schramm, and I. Iosilevskiy, Phys. Rev. C **88**, 014906 (2013).
[33] T. K. Herbst, J. M. Pawlowski, and B.-J. Schaefer, Phys. Rev. D **88**, 014007 (2013); Phys. Lett. B **696**, 58 (2011); E. Megías, E. R. Arriola, and L. L. Salcedo, Phys. Rev. D **74**, 065005 (2006); E. Megías, E. Ruiz Arriola, and L. L. Salcedo, Phys. Rev. D **74**, 114014 (2006); Eur. Phys. J. A **31**, 553 (2007).
[34] H. Ueda, T. Z. Nakano, A. Ohnishi, M. Ruggieri, and K. Sumiyoshi, Phys. Rev. D **88**, 074006 (2013).
[35] V. K. Tiwari, Phys. Rev. D **86**, 094032 (2012); arXiv:1301.3717v1.
[36] T. Kähärä and K. Tuominen, Phys. Rev. D **78**, 034015 (2008).
[37] G. Markó and Zs. Szép, Phys. Rev. D **82**, 065021 (2010).
[38] H. Mao, J. Jin, and M. Huang, J. Phys. G **37**, 035001 (2010).
[39] O. Lourenço, M. Dutra, A. Delfino, and M. Malheiro, Phys. Rev. D **84**, 125034 (2011).
[40] O. Lourenço, M. Dutra, T. Frederico, A. Delfino, and M. Malheiro, Phys. Rev. D **85**, 097504 (2012).
[41] S. Weissenborn, I. Sagert, G. Pagliara, M. Hempel, and J. Schaffner-Bielich, Astrophys. J. **740**, L14 (2011).
[42] G. Y. Shao, Phys. Lett. B **704**, 343 (2011).
[43] G. Lugones, T. A. S. do Carmo, A. G. Grunfeld, and N. N. Scoccola, Phys. Rev. D **81**, 085012 (2010); G. Lugones and A. G. Grunfeld, Phys. Rev. D **84**, 085003 (2011).
[44] J. G. Coelho, C. H. Lenzi, M. Malheiro, R. M. Marinho, Jr., and M. Fiolhais, Int. J. Mod. Phys. D **19**, 1521 (2010); C. H. Lenzi, A. S. Schneider, C. Providência, and R. M. Marinho, Jr., Phys. Rev. C **82**, 015809 (2010).
[45] M. Malheiro, M. Fiolhais, and A. R. Taurines, J. Phys. G **29**, 1045 (2003); J. G. Coelho, C. H. Lenzi, M. Malheiro, R. M. Marinho, Jr., C. Providência, and M. Fiolhais, Nucl. Phys. B, Proc. Suppl. **199**, 325 (2010); V. Dexheimer, J. Steinheimer, R. Negreiros, and S. Schramm, Phys. Rev. C **87**, 015804 (2013); N. S. Ayvazyan, G. Colucci, D. H. Rischke, and A. Sedrakian, arXiv:1308.3053.
[46] C. Höhne, K. E. Choi, V. Dobyrn *et al.*, Nucl. Instrum. Methods Phys. Res., Sect. A **639**, 294 (2011); P. Senger, T. Galatyuk, A. Kiseleva, D. Kresan, A. Lebedev, S. Lebedev, and A. Lymanets, J. Phys. G **36**, 064037 (2009); S. Chattopadhyay, J. Phys. G **35**, 104027 (2008); J. M. Heuser (CBM Collaboration), Nucl. Phys. **A830**, 563c (2009); http://www.gsi.de/fair.
[47] A. N. Sissakian, A. S. Sorin, and V. D. Toneev, arXiv:nucl-th/0608032; http://nica.jinr.ru/.
[48] V. A. Dexheimer and S. Schramm, Phys. Rev. C **81**, 045201 (2010); V. A. Dexheimer and S. Schramm, Nucl. Phys. **A827**, 579c (2009).
[49] B. W. Mintz, R. Stiele, R. O. Ramos, and J. Schaffner-Bielich, Phys. Rev. D **87**, 036004 (2013).
[50] L. McLerran and R. D. Pisarski, Nucl. Phys. **A796**, 83 (2007); L. Mclerran, Nucl. Phys. **A830**, 709c (2009);

L. McLerran, K. Redlich, and C. Sasaki, Nucl. Phys. **A824**, 86 (2009).

[51] N. Weiss, Phys. Rev. D **25**, 2667 (1982); K. Holland and U.-J. Wiese, *At The Frontier of Particle Physics - Handbook of QCD* (World Scientific, Singapore, 2001), Vol. 3, Chap. 32.

[52] K. Kashiwa, H. Kouno, M. Matsuzaki, and M. Yahiro, Phys. Lett. B **662**, 26 (2008); N. Bratovic, T. Hatsuda, and W. Weise, Phys. Lett. B **719**, 131 (2013); T. Hell, K. Kashiwa, and W. Weise, J. Mod. Phys. **4**, 644 (2013).

[53] K. Fukushima, Phys. Rev. D **78**, 114019 (2008).

[54] K. Kashiwa, H. Kouno, T. Sakaguchi, M. Matsuzaki, and M. Yahiro, Phys. Lett. B **647**, 446 (2007).

[55] F. Karsch, E. Laermann, and A. Peikert, Nucl. Phys. **B605**, 579 (2001); F. Karsch, Nucl. Phys. **A698**, 199 (2002); F. Karsch, Lect. Notes Phys. **583**, 209 (2002); O. Kaczmarek and F. Zantow, Phys. Rev. D **71**, 114510 (2005).

[56] Y. Sakai, T. Sasaki, H. Kouno, and M. Yahiro, Phys. Rev. D **82**, 076003 (2010).

[57] Y. Sakai, T. Sasaki, H. Kouno, and M. Yahiro, J. Phys. G **39**, 035004 (2012); M. Ferreira, P. Costa, D. P. Menezes, C. Providência, and N. Scoccola, arXiv:1305.4751v1.